

**Fig. 1. Schematic of the computational domain.**

transfer coefficient became a specially important variable for determining overall performance at high momentum flux ratios. Kusterer *et al.* (2007, 2009) proposed the double-jet film cooling technology to establish an anti-kidney vortex, which would prevent the double jet from lifting off the surface and raise the lateral spreading of the cooling air. Salimi *et al.* (2016) found that applying upstream jet film cooling configuration would have a significant improvement in the flow control capability and both centerline and span-wise averaged film cooling effectiveness. Sinha *et al.* (1991) studied the film cooling effectiveness with variable density ratio, it could be concluded that decreases in density ratio and increases in momentum flux ratio were found to reduce the spreading of the film cooling jet and reduce laterally averaged effectiveness. Qin *et al.* (2016) took the effects of streamwise pressure gradient and wall curvature into considerations on film cooling performance. Results showed that flow on the concave wall had an unstable effect and increases the turbulence intensity which led to a faster dissipation and wider lateral spreading. Bons *et al.* (1996) considered the effect of high freestream turbulence on film cooling effectiveness. Results showed that elevated levels of freestream turbulence reduced film cooling effectiveness by up to 70% in the region directly downstream of the injection hole due to enhanced mixing. Barlow and Kim (1995) reported that film effectiveness was reduced by smaller roughness elements more than larger elements, the presence of roughness apparently reduced the phenomena of "blow-off", which improved downstream effectiveness for the higher blowing ratios. Seo *et al.* (1998) presented the effect of length-to-diameter on heat transfer downstream of film cooling holes. Results indicated that the injectant velocity profiles became more uniform as the hole length increases. Burd *et al.* (1997) studied the influence of coolant supply geometry on film coolant exit flow and surface adiabatic effectiveness. It was found that the plenum geometry had an effect

on film cooling performance. Gritsch *et al.* (2003)

investigated the effect of internal coolant crossflow on the effectiveness of shaped film-cooling holes. The results showed that the film cooling effectiveness in the near hole region can be altered by over 100% for the crossflow cases compared to the plenum case.

Many investigations have been performed to understand the fundamental physics of film cooling. According to the coolant flow structure in the film cooling hole, the different ejection phenomena can produce different film cooling effectiveness. In this paper, heat transfer and cooling mechanism of film cooling with different coolant delivery configurations are conducted to improve the film cooling performance, seven delivery configurations with different contact angles between coolant chamber and film hole are designed to induce the various "jet phenomenon" in film cooling hole.

## 2. NUMERICAL MODEL

### 2.1 Geometric Configurations and Physical Model

The computational domain and geometries for different kinds of coolant delivery configurations are shown in Fig. 1 and Fig. 2. The calculation models are classified into four geometries which own the same dimensions of the mainstream and the film cooling hole configurations, a single cylindrical film cooling hole over a flat plate is adopted in this study. As shown in Fig. 2, the angle of  $\beta$  is defined firstly, and the clockwise direction is positive. The different coolant delivery configurations with various contact angles between the coolant plenum and the film cooling hole which the  $\beta$  is ranging from  $-45^\circ$  to  $+30^\circ$  are considered in this research, and the  $\beta$  is  $-60^\circ$  for reference case. As shown in figure, the diameter of the film cooling hole ( $D$ ) is 8 mm which injects the coolant inclined to the mainstream direction with an angle of  $30^\circ$ . The computational domain has dimensions of  $10D \times 40D \times 15D$ , the film cooling hole spacing ratio ( $P/D$ ) is equal to 3.

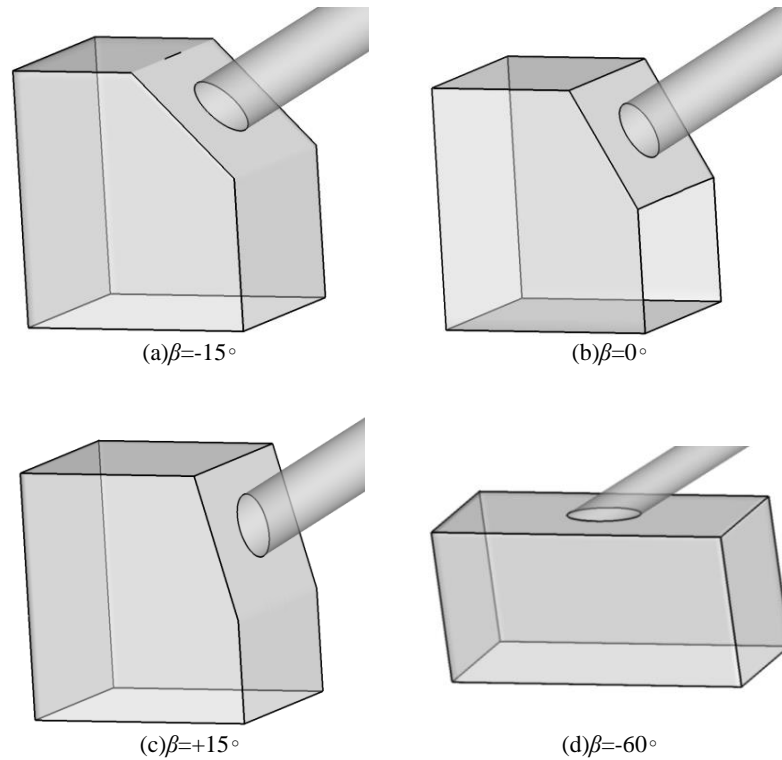


**Fig. 2. Geometries for different kinds of coolant delivery configurations.**

Structured meshes are employed for the numerical simulations of different coolant delivery configurations, the details of the structured grids related to the computational domain are shown in Fig. 3. The boundary layer mesh near the no-slip wall is generated to achieve the requirements of the turbulence model. By comparing the results with the different ascending nodes, when the grid number of 1.2 million nodes is reached, the centerline effectiveness of film cooling wall is matches very well and any more additional grids will give the same result. Hence, the grid number of 1.2 million nodes is selected for all simulations.

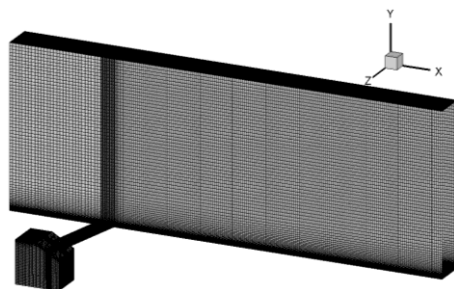


**Fig. 3. Schematic of mesh.**

## 2.2 Boundary Conditions and Operating Parameters

Boundary conditions of the different kinds of coolant delivery configuration are indicated in Fig. 1, the high temperature free stream enters the main duct domain with fixed inlet velocity (20 m/s) and

total temperature of (300K) at 5% of turbulence intensity, while the cooling fluid enters the plenum at a constant total temperature of (150K) and 1% of turbulence intensity to achieve a constant value of the density ratio ( $DR=2$ ) for all cases. The inlet velocity of the coolant varies according to the used values of the blowing ratios, the outlet boundary condition is set at an average static pressure of 1 atm. The upper surface of the main duct is used as a free-slip adiabatic wall and the two opposite side surfaces of the same duct are set as translational periodicity interface condition. The other surfaces of the full computational domain are treated as a no-slip adiabatic wall.

The numerical simulations of different coolant delivery configurations are conducted with ANSYS CFX 17.0. The high resolution is selected for advection scheme and turbulence numerics, wherein the convergence criteria for the steady solution is set of  $1e-6$  for all terms; mass, three components of velocity, energy and turbulence model. The solution is believed to be converged when it reached to the residual target  $1e-6$  for all terms and mass and energy imbalance percentage less than 0.05%.

## 2.3 Turbulence Model

For heat transfer and flow-field computational modeling with different coolant delivery configurations, the numerical results are dependent on the turbulence model. The film cooling experiment conducted by *Sinha et al. (1991)* is adopted to verify the numerical method. Four turbulence models (shear stress transport SST,  $k-\omega$ , RNG  $k-\epsilon$  and standard  $k-\epsilon$ ) are selected in this paper. The numerical simulation is conducted using

those turbulence models and the results are compared to the experimental data under the same operating conditions to verify the turbulence model. Figure 4 illustrates the centerline adiabatic effectiveness distributions along the streamwise direction for the four turbulence models and the experimental data. The Shear-Stress-Transport (SST) model results could predict very well the experimental data than the other turbulence models. As a result, Shear-Stress-Transport (SST) model is selected to simulate the film cooling process for all different cases in this paper (2015).

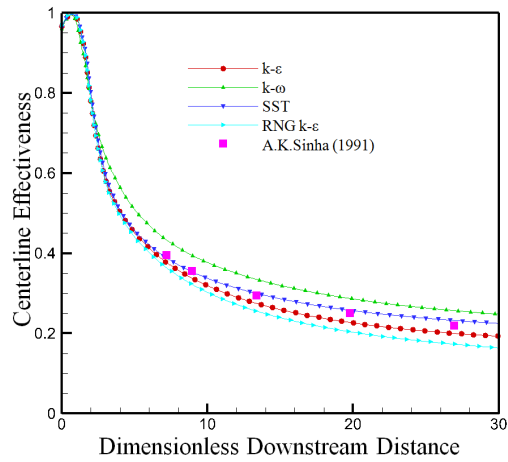


**Fig. 4. Comparison between numerical results and experiment dates.**

## 2.4 The Definition of Parameters

The definition of blowing ratio is given as:

$$M = \rho_c V_c / (\rho_\infty V_\infty) \quad (1)$$

In the Equation,  $\rho_c$  is the density of coolant air,  $\rho_\infty$  is the density of freestream,  $V_c$  is the average inlet velocity of the coolant air,  $V_\infty$  is the velocity of freestream.

The definition of the adiabatic film cooling effectiveness  $\eta$  is defined as:

$$\eta = (T_g - T_{aw}) / (T_g - T_c) \quad (2)$$

In above equation,  $T_{aw}$  is the adiabatic temperature of the cooling wall,  $T_g$  is the temperature of freestream,  $T_c$  is the temperature of coolant air.

The definition of the average adiabatic film cooling effectiveness  $\bar{\eta}$  is:

$$\bar{\eta} = \frac{1}{\Delta z} \int \eta(x, z) dz \quad (3)$$

In above equation, the flow direction is the  $x$  axis, and spanwise direction is  $z$  axis.

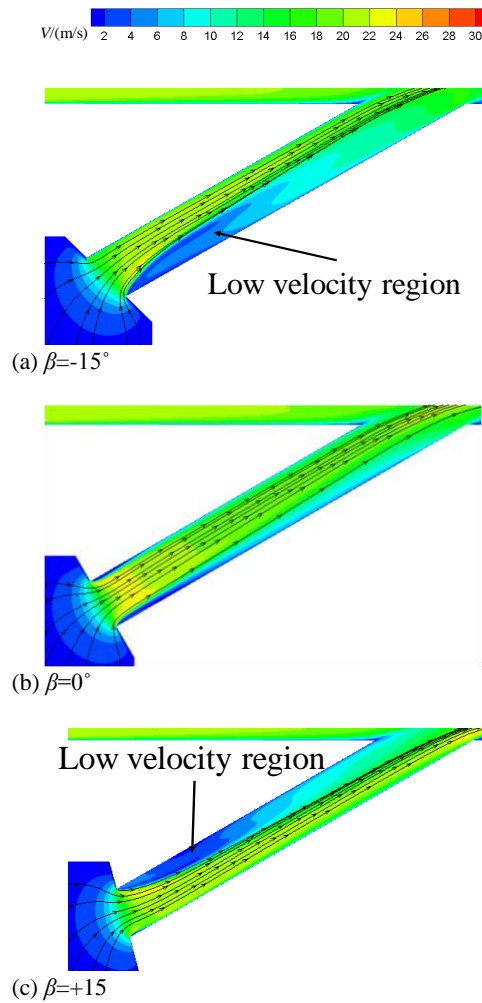


**Fig. 5. Contour of velocity and stream line pattern at mid plane in film hole ( $M=1.5$ ).**

## 3. NUMERICAL RESULTS AND DISCUSSION

### 3.1 Flow Field Analysis inside the Film Hole

The fluid field characteristic inside the film cooling hole is introduced to discuss the major factors affecting the flow-field to understand the physical phenomena for each coolant delivery configuration model, and it is mainly affected by hole shape, coolant delivery configuration and blowing ratio. The effect of different coolant delivery configurations (different angles of  $\beta$ ) on flow field characteristics is studied at the blowing ratio  $M = 1.5$  in this section. As shown in Fig. 5, the three most representative angles for  $\beta = -15^\circ, 0^\circ, +15^\circ$  are selected to analyze the flow field characteristics for different coolant delivery configurations, it can be very obvious seen the difference of flow field characteristics from the magnitude velocity contours with streamlines at a part of the mid-section  $x$ - $y$  plane in the film cooling hole for each model under the same aforementioned classification of blowing ratios. The direction of coolant into the film hole is basically the same as that of the hole

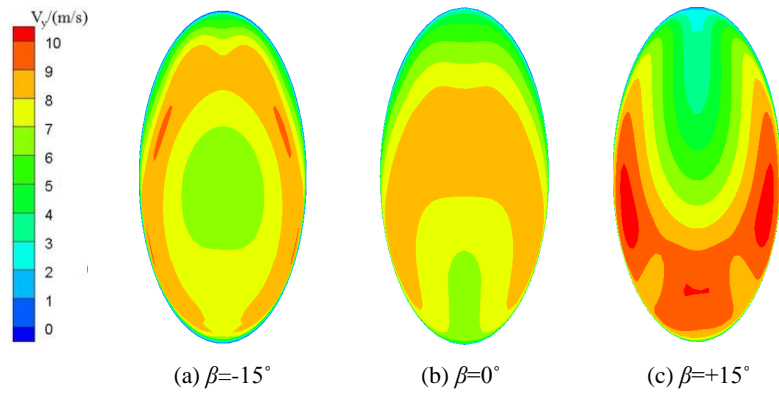


**Fig. 6. Contour of  $V_y$  at the exit of film cooling hole ( $M=1.5$ ).**

axis when the  $\beta$  is  $0^\circ$ . The angle between coolant direction and hole axis is occurred when the angle is  $\beta \neq 0^\circ$ , coolant entering the film cooling hole will cause the injection phenomenon. Part of the coolant enters film cooling hole with acute angle  $\delta$  between the flow direction and the hole axis (as shown in the upper left part of the contact location between the coolant plenum and the film hole). It is equivalent to shrinking surface to accelerate the coolant. Another part of the coolant enters film cooling hole with obtuse angle  $\delta$  between the flow direction and the hole axis (as shown in the lower right part of the contact location between the coolant plenum and the film hole). It is equivalent to expanding surface to slow down the coolant. The high momentum zone and low momentum zone are formed by the acceleration and separation of the fluid flow at inlet of film cooling hole. The distribution of velocity and pressure at the exit of film cooling hole would be affected by these flow field characteristics.

The magnitude velocity contours distribution in  $y$  directions at exit of film cooling hole are presented in Fig. 6, and the coolant component velocity in  $y$  direction determines the ability to penetrate the main flow boundary layer. As shown in the figure, the location of low velocity region is different for various coolant delivery configurations. The low velocity region is located at the downstream of the film hole exit when the  $\beta$  is  $-15^\circ$ . On the contrary, it is located at the upstream of the film hole exit when the  $\beta$  is  $+15^\circ$ . When the angle of  $\beta$  is  $0^\circ$ , the velocity distribution looks like more uniform. The velocity distribution characteristics induced by different coolant delivery configurations has a significant impact on film cooling effectiveness.

Figure 7 shows the static pressure distributions on at mid plane and exit of film hole ( $\beta=0^\circ$ ). The high and the low-pressure region are formed at the upstream and downstream of film hole exit due to the interaction between mainstream and film cooling injection. The favorable pressure gradient can be observed on the film hole exit, which will increase the velocity of the coolant downstream of the film hole. It also has an important impact on vortex structure outside the film cooling hole.

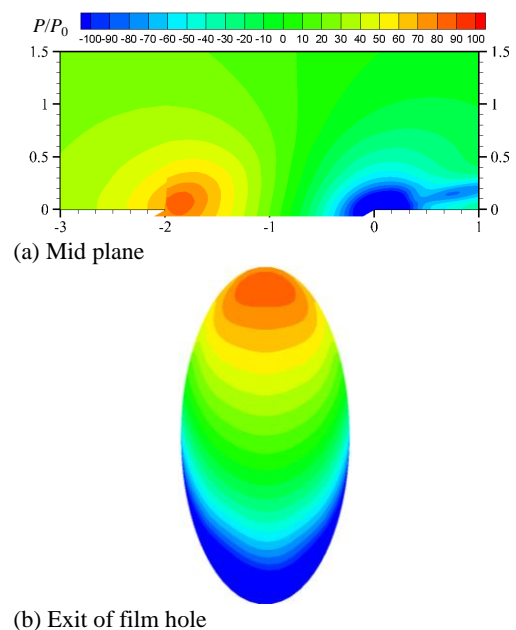


**Fig. 7. Static pressure contours on at mid plane and exit of film hole ( $\beta=0^\circ$ ).**

### 3.2 Flow Field Analysis outside the Film Hole

The temperature contours with streamlines for the different studied models on the cross sections at the downstream of film cooling hole are shown in Fig. 8. The kidney vortex is formed near the exit of film-hole which grows downstream as a strong vortex with small domain near the target surface and become wider and weaker in further downstream as shown in the different sections. As shown in Fig. 8, the coolant injection moves away from the wall in the vertical direction for  $\beta=-30^\circ$  and  $\beta=0^\circ$ , and it could not protect the cooling wall very well. However, a contour of the temperature distribution whose shape is like the "nose" is formed for  $\beta=30^\circ$ , which shows a big different with the typical kidney vortex structure. The distance between vortex core for kidney vortex pairs is larger than  $\beta=-30^\circ$  and  $\beta=0^\circ$ , the coolant injection moves towards to the wall to provide a better cooling film coverage at the downstream of the cross sections.

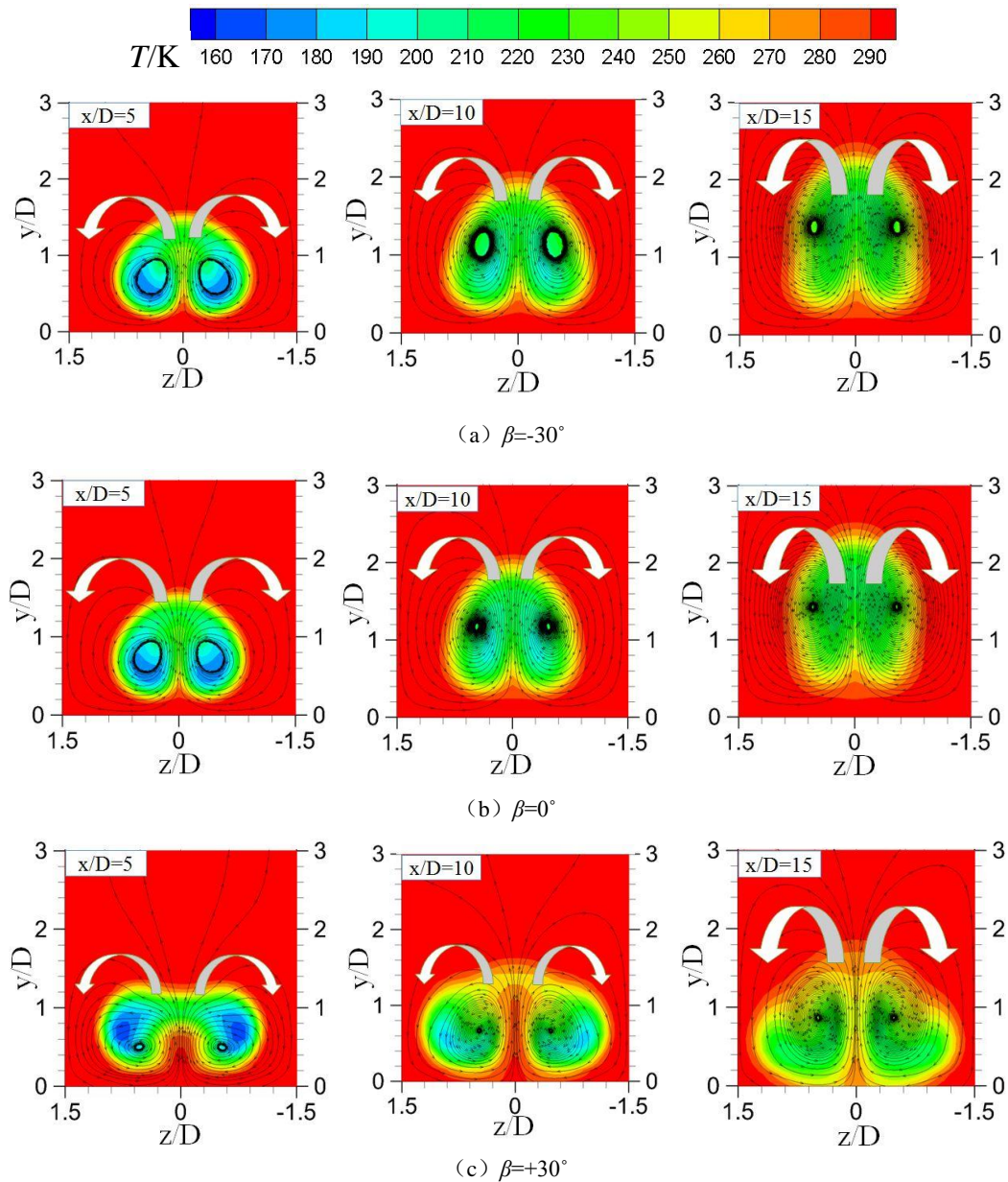


**Fig. 8. Temperature contours and streamlines on the cross sections at the downstream of film hole.**

Figure 9 shows the coolant path lines started from the film hole and colored by the velocity magnitude ( $M=2.0$ ). The difference of flow field distribution for three kinds of coolant delivery configurations is obvious. The coolant injection is lifted from film cooling wall due to the higher momentum for  $\beta=-30^\circ$  and  $\beta=0^\circ$ , the different flow field characteristics can be seen for  $\beta=+30^\circ$ , part of cooling air at two side of injection zone interacts with mainstream, and the upstream cooling air in low momentum zone bypasses the large jet momentum cooling air to attach cooling surface at downstream, this part of cooling air is corresponding to that of low velocity region in Fig. 6. This flow characteristic can improve the film cooling performance at the downstream of cooling wall, especially for high blowing ratio.

The temperature distributions on  $xy$  plane ( $z=0$ ) for

blowing ratio  $M=2.0$  are presented in Fig.10 for three kinds of coolant delivery configurations. The primary process by which film cooling reduces the heat transfer to the wall is by reducing the gas temperature near the wall. As shown in Fig. 10a and 10b, coolant jets that were fully detached for  $\beta=-15^\circ$  and  $\beta=0^\circ$  at blowing ratio  $M=2.0$ . The coolant jet separation characteristics were found to scale with momentum flux ratio between coolant jet and mainstream. This is understandable because the dynamics of the force of the mainstream impacting the coolant jet and causing it to turn toward the wall would be expected to be primarily a function of the momentum of the coolant jet relative to the momentum of the mainstream. However, the coolant jets initially detached but soon reattached to the cooling surface for  $\beta=+30^\circ$ , it could provide a better cooling performance.

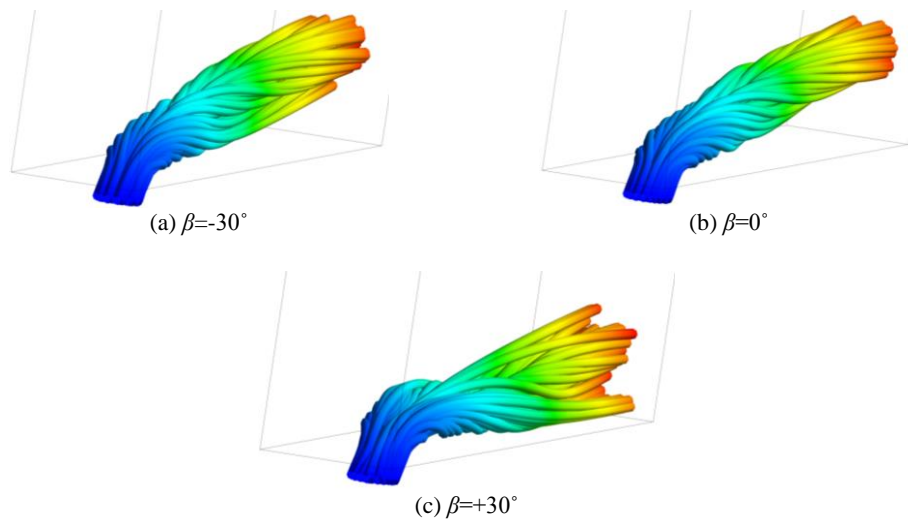


**Fig.9.** Pathlines started from the film hole and colored by the velocity magnitude( $M=2.0$ ).

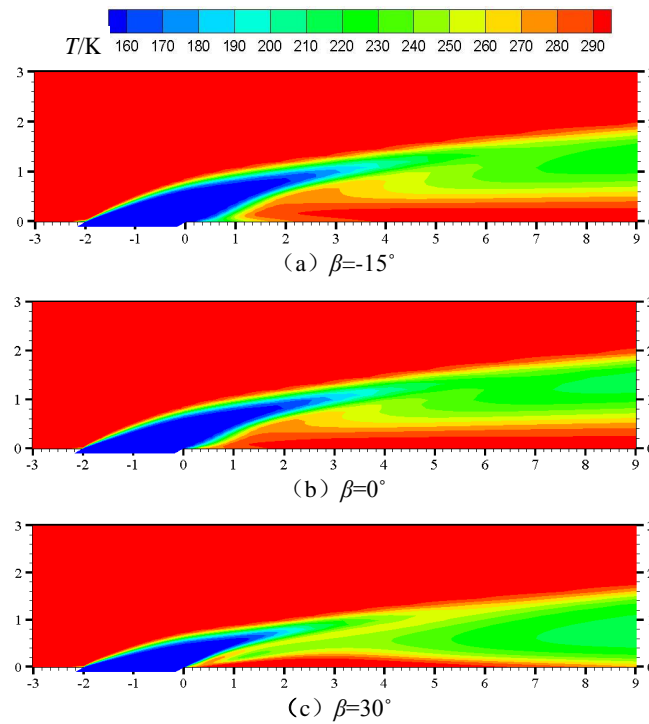


**Fig.10.** Temperature distribution on  $xy$  plane ( $z=0$ ) for blowing ratio  $M=2.0$ .

### 3.3 Cooling Effectiveness

Adiabatic film cooling effectiveness distribution at different streamwise locations for  $M=2.0$  is given in Fig. 11. Two peak values of adiabatic film cooling effectiveness can be seen for the positive  $\beta$  cases, and the peak value locates at  $z/D=\pm 0.5$ . On the other hand, the adiabatic film cooling effectiveness of  $\beta=+30^\circ$  is less than other cases at  $x/D=5$ , however, it shows an extremely higher adiabatic film cooling effectiveness of  $\beta=+30^\circ$  than other cases at  $x/D=10$  and  $x/D=15$ . It can be concluded that coolant delivery configuration with  $\beta=+30^\circ$  could improve the downstream adiabatic film cooling effectiveness on cooling wall. Figure 12 presents the adiabatic

film cooling effectiveness distribution at different blowing ratios ( $x/D=10$ ). For a certain streamwise location, the distribution of adiabatic film cooling effectiveness is quite different for various blowing ratios. Two peak values of adiabatic film cooling effectiveness only appear at high blowing ratio, and the position of the peak moves to center line with the decreasing of blowing ratio.

Figure 13 and Fig. 14 show contours of the local adiabatic film cooling effectiveness on cooling surface of different coolant delivery configurations for the blowing ratios of 0.5 and 1.5. With the blowing ratio of 0.5, three kinds of coolant delivery configurations yield similar contour shapes, but the

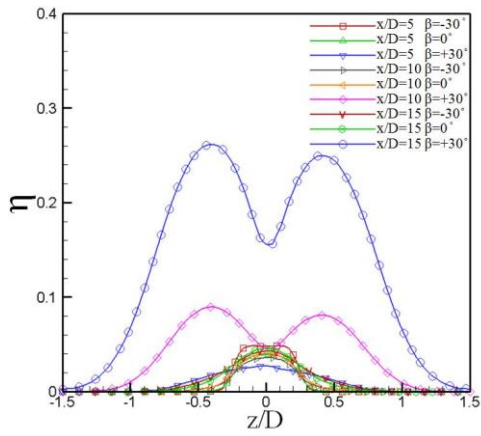


**Fig. 11.** Adiabatic film cooling effectiveness distribution at different streamwise locations ( $M=2.0$ ).

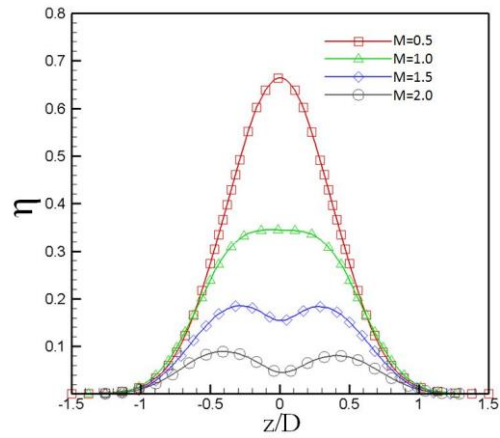


**Fig. 12.** Adiabatic film cooling effectiveness distribution at different blowing ratios ( $x/D=10$ ).

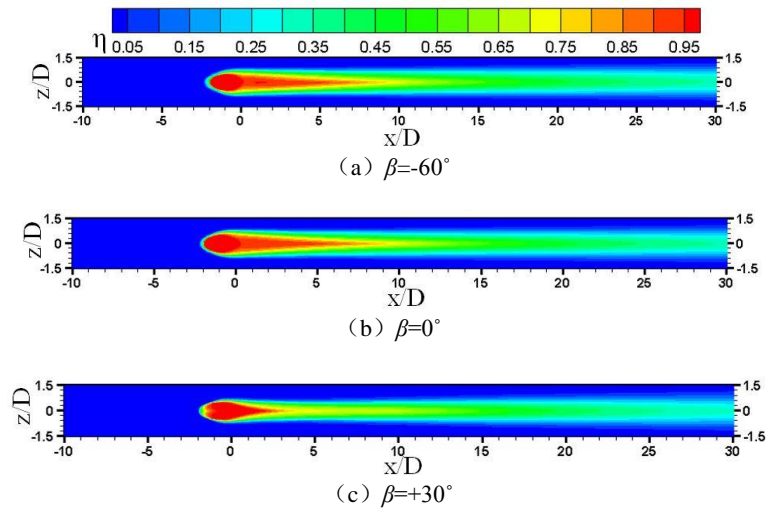


**Fig. 13.** Adiabatic cooling effectiveness contours of different coolant delivery configurations at  $M=0.5$ .

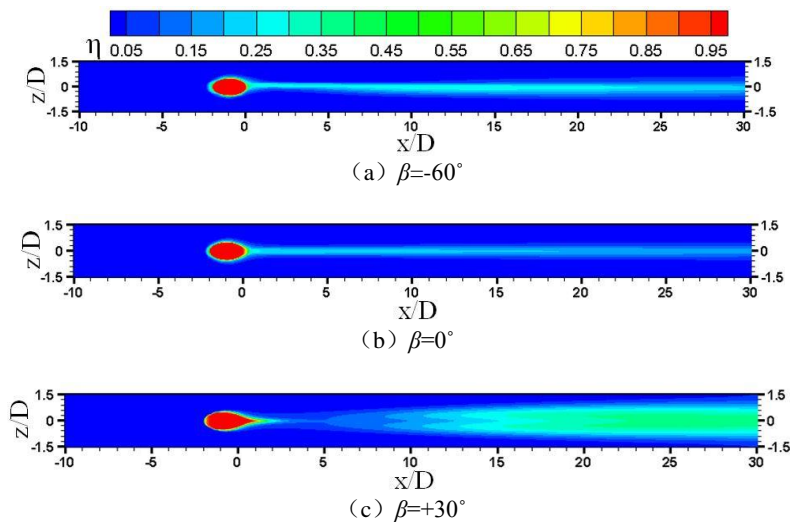


**Fig. 14.** Adiabatic cooling effectiveness contours of different coolant delivery configurations at  $M=1.5$ .

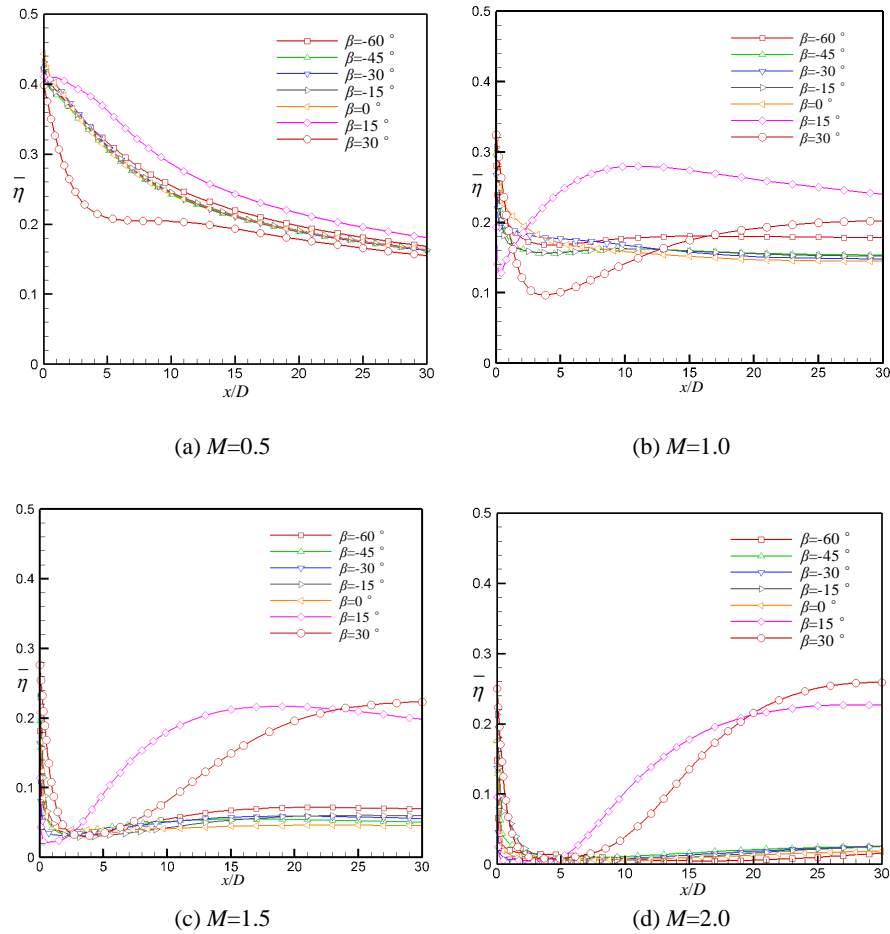


**Fig. 15. Average adiabatic film cooling effectiveness of different coolant delivery configurations along  $x$  direction for varying blowing ratios.**

coolant delivery configuration with  $\beta=+30^\circ$  shows a less lateral spreading region of high film cooling effectiveness. At a blowing ratio of 1.5, the adiabatic film cooling effectiveness is very low for coolant delivery configurations of  $\beta=-60^\circ$  and  $\beta=0^\circ$  due to the coolant jet separating from the surface.

However, in the downstream region of the film cooling surface where lower adiabatic film cooling effectiveness generally occurs at high blowing ratio, the coolant delivery configurations of  $\beta=+30^\circ$  shows high adiabatic film cooling effectiveness at downstream of cooling surface. The reason is that the coolant in this case interacts with high temperature mainstream, and the coolant in the low momentum region of upstream bypasses the large jet momentum coolant to attach cooling surface at downstream. It could increase the distance between the vortexes to weaken mutually reinforcing effect, so coolant delivery configuration of  $\beta=+30^\circ$  shows a very higher adiabatic film cooling effectiveness than other case. Clearly, whether the coolant jets are attached strongly affects the cooling performance.

Figure 15 shows average adiabatic film cooling

effectiveness of different coolant delivery configurations along  $x$  direction for varying blowing ratios. For the blowing ratios of 0.5 and 1.0, the coolant delivery configurations with  $\beta=+30^\circ$  appears to collapse of average adiabatic film cooling effectiveness around  $x/D=5$ , and the coolant delivery configurations with  $\beta=+15^\circ$  shows the highest average adiabatic film cooling effectiveness except the upstream of  $M=1.0$ . For the blowing ratios of 1.5 and 2.0, the extremely high average adiabatic film cooling effectiveness is appeared for both  $\beta=+15^\circ$  and  $\beta=+30^\circ$ . It also can be concluded that the reattached position of  $\beta=+30^\circ$  moves towards downstream of cooling surface. When the blowing ratio is 1.5, the average adiabatic film cooling effectiveness of  $\beta=+15^\circ$  and  $\beta=+30^\circ$  in the calculated region ( $0 \leq x/D \leq 30$ ,  $-1.5 \leq z/D \leq 1.5$ ) is increased by about 130% and 70% compared to case of  $\beta=-60^\circ$ , respectively. When the blowing ratio is increased from 1.5 to 2.0, the increase of average adiabatic film cooling effectiveness is about 310% and 300%.

#### 4. CONCLUSION

Heat transfer and cooling mechanism of film cooling with different coolant delivery configurations are conducted to improve the film cooling performance in this paper, seven delivery configurations with different contact angles between coolant chamber and film hole are investigated. Conclusions can be drawn as follows:

- (1) The outlet velocity distribution of the film cooling hole is mainly affected by the flow structure in film cooling hole and the interactions between the coolant jet and the main flow. The high and the low-pressure region are formed at the upstream and downstream of film hole exit due to the interactions between mainstream and film cooling injection. The favorable pressure gradient can be observed on the film hole exit, which will increase the velocity of the coolant downstream of the film hole.
- (2) At high blowing ratio, the strong kidney-shaped vortex is formed outside the film cooling hole causing a low cooling effectiveness for  $\beta \leq 0^\circ$ . For  $\beta > 0^\circ$ , the coolant interacts with high temperature mainstream, and the coolant in the low momentum region of upstream bypasses the large jet momentum coolant to attach cooling surface at downstream. It increases the distance between the vortices to weaken mutually reinforcing effect, resulting in high film cooling effectiveness. The reattached position moves towards to downstream with the increase of the blowing ratio, and it moves backward as the  $\beta$  increased.
- (3) When the blowing ratio is 1.5, the average adiabatic film cooling effectiveness of  $\beta = +15^\circ$  and  $\beta = +30^\circ$  in the calculated region ( $0 \leq x/D \leq 30$ ,  $-1.5 \leq z/D \leq 1.5$ ) is increased by about 130% and 70% compared to case of  $\beta = -60^\circ$ , respectively. When the blowing ratio is increased from 1.5 to 2.0, the increase of average adiabatic film cooling effectiveness is about 310% and 300%.

#### ACKNOWLEDGEMENTS

The authors wish to thank the support of National Natural Science Foundation of China (No. 51809065), Fundamental Research Funds for the Central Universities (No: 3072020CF0302, No: 3072020CFT1504).

#### REFERENCES

Barlow, D. N. and Kim, Y. W (1995). Effect of surface roughness on local heat transfer and film cooling effectiveness. *International Gas Turbine and Aeroengine Congress and*

*Exposition*, 95-GT-14.

- Bons, J. P., C. D. MacArthur and R. B. Rivir (1996). The effect of high free-stream turbulence on film cooling effectiveness. *Journal of Turbomachinery* 118(4), 814-825.
- Bunker, R. S. (2005). A review of shaped hole turbine film-cooling technology. *Journal of Heat Transfer* 127(4), 441-453.
- Bunker, R. S. (2006). Gas turbine heat transfer: 10 remaining hot gas path challenges. *Proceedings of ASME Turbo Expo*, GT2006-90002.
- Burd, S. W. and T. W. Simon (1997). The influence of coolant supply geometry on film coolant exit flow and surface adiabatic effectiveness. *International Gas Turbine and Aeroengine Congress and Exhibition*, 97-GT-25.
- Gritsch, M., A. Schulz and S. Wittig (2003). Effect of internal coolant crossflow on the effectiveness of shaped film-cooling holes. *Journal of Turbomachinery* 125(3) 547-554.
- Han, J. C., S. Dutta and S. Ekkad (2013). *Gas turbine heat transfer and cooling technology*, CRC press, New York.
- Jiang, Y. T., H. F. Lin, G. Q. Yue, Q. Zheng, and X. L. Xu (2017). Aero-thermal optimization on multi-rows film cooling of a realistic marine high pressure turbine vane. *Applied Thermal Engineering* 111, 537-549.
- Jiang, Y. T., Q. Zheng, P. Dong, J. H. Yao, H. Zhang, and J. Gao (2015). Conjugate heat transfer analysis of leading edge and downstream mist-air film cooling on turbine vane. *International Journal of Heat and Mass Transfer* 90, 613-626.
- Kusterer, K., A. Elays, D. Bohn, T. Sugimoto, R. Tanaka, and M. Kazari (2009). A parametric study on the influence of the lateral ejection angle of double-jet holes on the film cooling effectiveness for high blowing ratios. *Proceedings of ASME Turbo Expo*, GT2009-59321.
- Kusterer, K., A. Elays, D. Bohn, T. Sugimoto, and R. Tanaka (2007). Double-jet ejection of cooling air for improved film cooling. *Journal of Turbomachinery* 129(4), 809-815.
- Lee, K. D. and K. Y. Kim (2009). Optimization of a cylindrical film cooling hole using surrogate modeling. *Numerical Heat Transfer, Part A: Applications* 55(4), 362-380.
- Qin, Y. M., P. T. Chen, J. Ren, and H. D. Jiang (2016). Effects of wall curvature and streamwise pressure gradient on film cooling effectiveness. *Applied Thermal Engineering* 107, 776-784.
- Salimi, M. R., M. Ramezanizadeh, M. Taeibi-Rahni, and R. Farhadi-Azar (2016). Film cooling effectiveness enhancement applying another jet in the upstream neighbor of the

- main jet-using les approach. *Journal of Applied Fluid Mechanics* 9(1), 33-42.
- Schmidt, D. L., B. Sen and D. G. Bogard (1994). Film cooling with compound angle holes: adiabatic effectiveness. *International Gas Turbine and Aeroengine Congress and Exposition*, 94-GT-312.
- Sen, B., D. L. Schmidt and D. G. Bogard (1994). Film cooling with compound angle holes: heat transfer. *International Gas Turbine and Aeroengine Congress and Exposition*, 94-GT-311.
- Seo, H. J., J. S. Lee and P. M. Ligrani (1998). Effects of bulk flow pulsations on film cooling from different length injection holes at different blowing ratios. *International Gas Turbine and Aeroengine Congress and Exhibition*, 98-GT-192.
- Sinha, A. K., D. G. Bogard and M. E. Crawford (1991). Film cooling effectiveness downstream of a single row of holes with variable density ratio. *Journal of Turbomachinery* 113(3), 442-449.